Supplementary Information for

Carbon Nanotube Yarn based Thermoelectric Textiles for Harvesting Thermal Energy and Powering Electronics

Yuanyuan Zheng[1], Qihao Zhang[2], Wenlong Jin[3], Yuanyuan Jing[1], Xinyi Chen[1], Xue Han[1], Qinye Bao[4], Yanping Liu[1], Xinhou Wang[1], Shiren Wang[5], Yiping Qiu[1,6], Chong-an Di[3*], Kun Zhang[1*]

[1]Key Laboratory of Textile Science & Technology (Ministry of Education), College of Textiles, Donghua University, Shanghai 201620, PR China

[2]State Key Laboratory of High Performance Ceramics and Superfine Microstructure, Shanghai Institute of Ceramics, Chinese Academy of Sciences, Shanghai, 200050, China

[3]Beijing National Laboratory for Molecular Sciences, Key Laboratory of Organic Solids, Institute of Chemistry, CAS, Beijing 100190, China

[4]Key Laboratory of Polar Materials and Devices, Ministry of Education, School of Information Science Technology, East China Normal University, 200241, Shanghai, P. R. China

[5]Department of Industrial and Systems Engineering, Texas A&M University, College Station, TX 77843, United States

[6]College of Textiles and Apparel, Quanzhou Normal University, Fujian 362000, China

[*]Corresponding authors: K.Z. (email: kun.zhang@dhu.edu.cn), and C.D. (email: dicha@iccas.ac.cn)

Contents

Supplementary Figure 6 | The simulated thermoelectric output voltage of bared single p-n pair of TEY.

Supplementary Figure 7 | The simplified thermal resistance model.

Supplementary Figure 8 | The simulation and experimental results of spacer fabric based TET.

Supplementary Figure 9 | The effect of fabric thickness of spacer fabric on the thermoelectric power generation of TET.

Supplementary Figure 10 | Stability of **a.** electrical resistance and **b.** Seebeck coefficient of TET under twisting, bending, compression and stretching.

Supplementary Figure 11 | Demonstration of as-prepared TET powering several typical electronics including **a.** thermometer, **b.** thermo-hygrometer, **c.** UV detector and **d.** pedometer (ΔT~40 K).

Supplementary Figure 12 | The measurement diagram of power generation during the powering electronics process (ΔT between the top and bottom surface of TET is ~40 K).

Supplementary Figure 13 | Demonstration of scalable manufacturing weft-knitted spacer fabric based TETs.

Supplementary Figure 14 | Lapping diagram of TEY and textile yarn.

Supplementary Figure 15 | The temperature-dependent electrical conductivity of pure CNTY.

Supplementary Table 1 Thermoelectric properties (electrical conductivity(σ), Seebeck coefficient (*S*) and power factor (PF)) of as-purchased CNTY.

Supplementary Notes

Supplementary Note 1

The preparation of pure CNT film and PEI-doped CNT film

The pure CNT films were purchased from Suzhou Xiyin nanotechnology company. The pure CNT films were spin coated on a clean indium tin oxide (ITO) glass substrate with a size of 10 mm×6 mm×~50 nm in which the kind of multi-walled carbon nanotubes (MWCNTs) is the same as the MWCNTS in CNTY. For the PEI-CNT film, the concentration of PEI in ethanol is 0.8 mM. Each PEI/CNT film contains 1 ul PEI/ethanol solution.

Supplementary Note 2

Thermo-wet comfortability of TET

The air Permeability was measured by YG461H fully automatic permeability instrument (fabricated by NINGBO textile instrument factory) according to GB/T 11048-2008.

Supplementary Table 7 shows that all measured parameters referring to the thermo-wet comfort are very similar to the as-received spacer fabric and TET, indicating little effect of incorporated TEY on the wearing performance. The air permeability of TET is 10% lower than that of the spacer fabric. The thermal resistance and Clo value of TET are increased by 9.7% as compared with that of untreated warp-knitted spacer fabric. After threading the TEY into the spacer fabric, the heat transfer coefficient is 91.1% of that of spacer fabric, indicating a better thermal insulation

performance.

Supplementary Note 3

Design parameters and knitting process of weft-knitted spacer fabric shaped TET using TEYs

Needle setting: 66;

Yarn: nylon/spandex covered yarns×2 (70D/20D), polyester monofilament (0.12 mm).

1. Technical Parameters:

Machine: ADF 530-32W, Stitch length 7.2, Needle hook gauge 10;

Stitch length: Top and bottom layer plain 11.5, polyester monofilament tuck 8.6, investigated yarn tuck 9;

Speed: 0.5 m/s, (peed is slowed down by manual control during actual knitting)

fabric take-up: 1.7.

During the knitting process, the yarn was periodically fed into the computerized flat knitting machine (ADF 530-32 W, Germany Stoll) as spacer yarns to form weft-knitted spacer fabrics using two sets of needles. Weft-knitted spacer fabrics consist of two separate outer knitted layers interconnected by spacer yarns. Producing spacer fabrics on flat machines is creating two independent fabric layers on the front- and back-needle beds separately and then connecting them by tucks on both the needle beds. The distance between the two needle beds determines the thickness of spacer fabric, which can be finely tuned to match the CNT yarn based thermoelectric legs. The specific knitting process is as follows: first, the yarns are knitted on the front and back needle

bed to form a row of needles with the top outer layer and the bottom outer layer, respectively. Then the yarn is knitted on the front and back needle bed at the same time. Finally, spacer fabrics with 14 needle spacing are knitted on the machine.

We notify that the knitting fabric shows relatively higher thermoelectric output power as the fabric weight and height are the same. Honestly, it is much easier to fabricate thick spacer fabrics (up to 30cm thick) than other types of textiles. Moreover, it is clearly to monitor the moving track of CNT yarn during knitting process.

Supplementary Figures

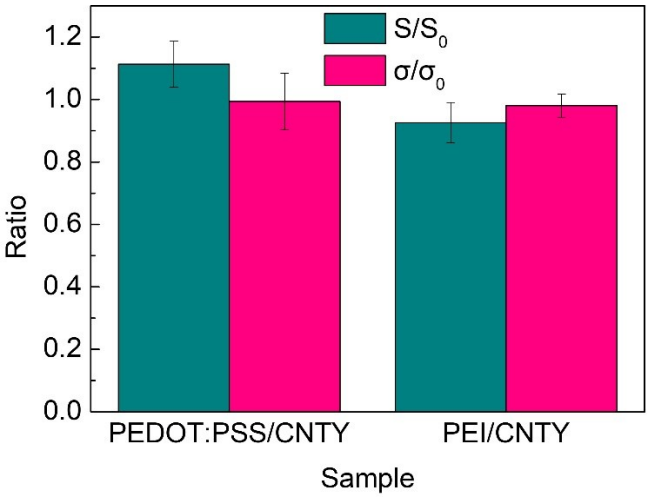

Supplementary Figure 1 | Air stability of the Seebeck coefficients and electrical conductivities of PEDOT:PSS and PEI doped CNT yarn (S_0 and σ_0 are the initial Seebeck coefficient and electrical conductivity of PEDOT:PSS and PEI doped CNT yarn; S and σ are the Seebeck coefficient and electrical conductivity of PEDOT:PSS and PEI doped CNT yarn after 14 days in ambient environment).

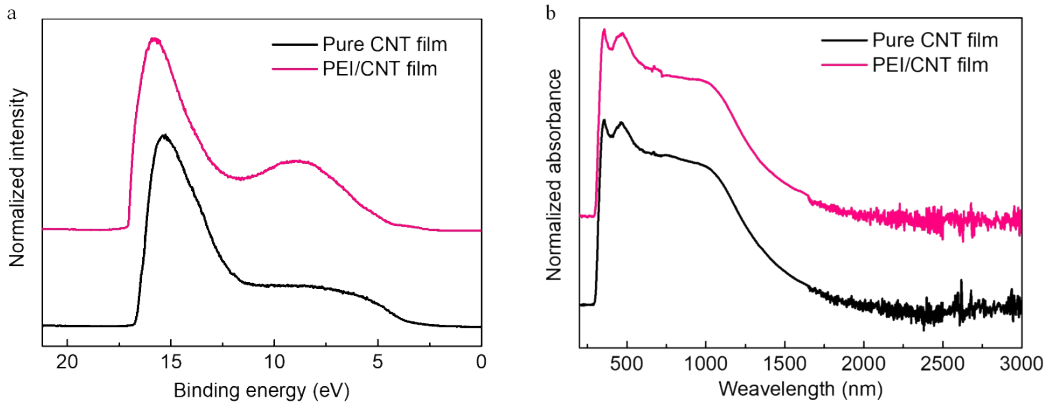

Supplementary Figure 2 | The full spectra of **a.** UPS and **b.** UV-Vis of pure CNT film and PEI/CNT film.

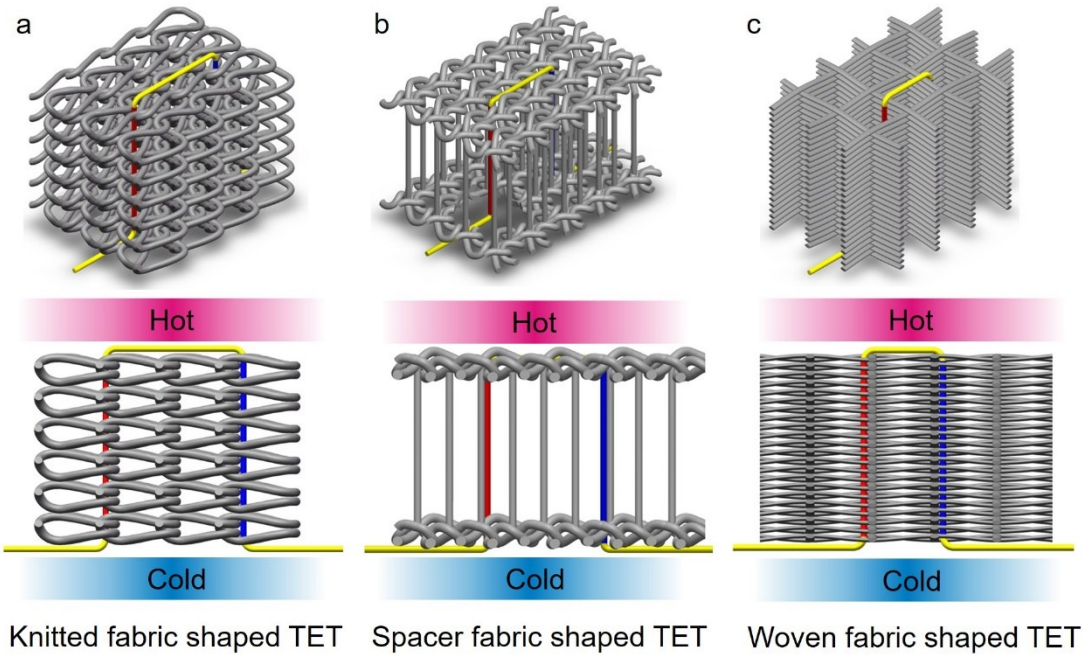

Supplementary Figure 3 | The operation principle and diagrams of **a.** knitted fabric shaped TET, **b.** spacer fabric shaped TET and **c.** woven fabric shaped TET. In the three diagrams, the gray part is the textile substrate, the red part is p-type leg, the blue part is n-type leg and the yellow part is the electrode.

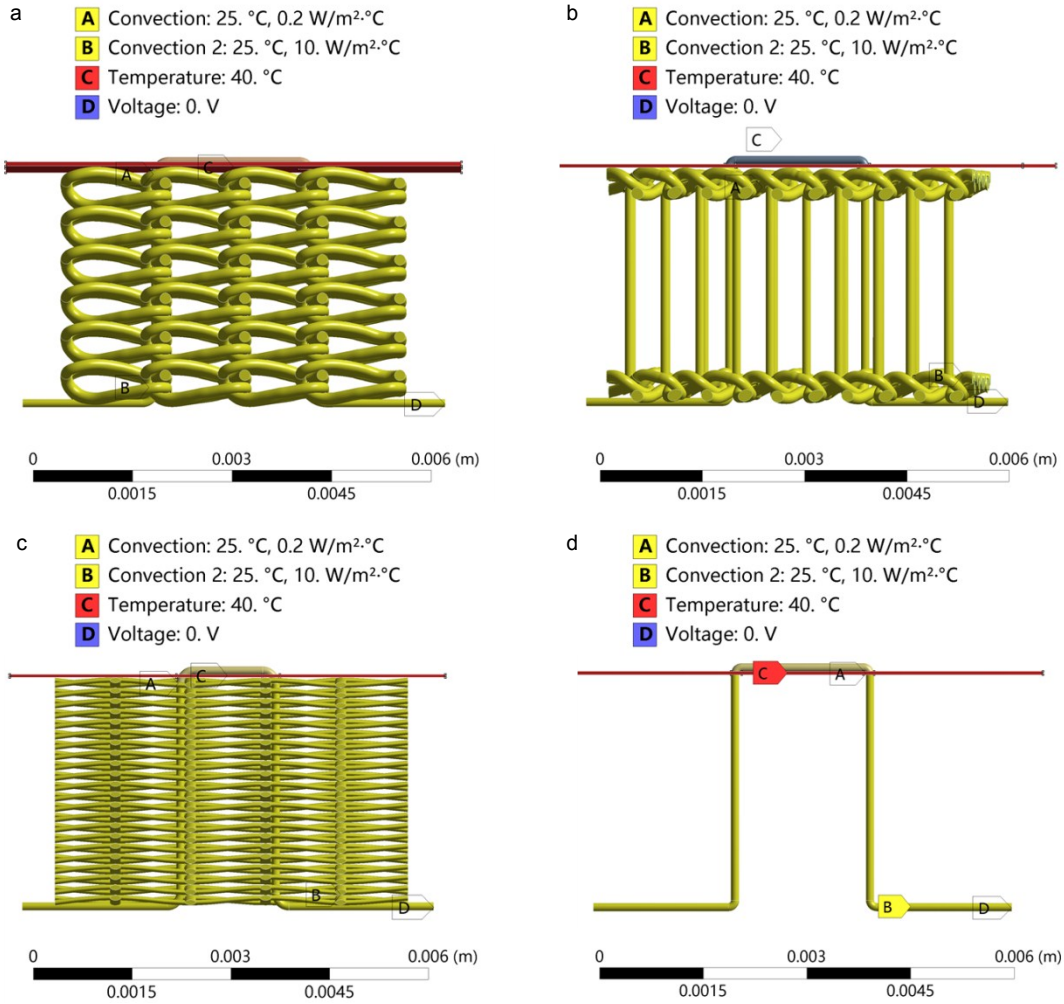

Supplementary Figure 4 | Detailed boundary conditions applied in the finite element analysis. **a.** Knitted fabric shaped TET. **b.** Spacer fabric shaped TET. **c**. Woven fabric shaped TET. **d.** Bared single p-n pair of TEY.

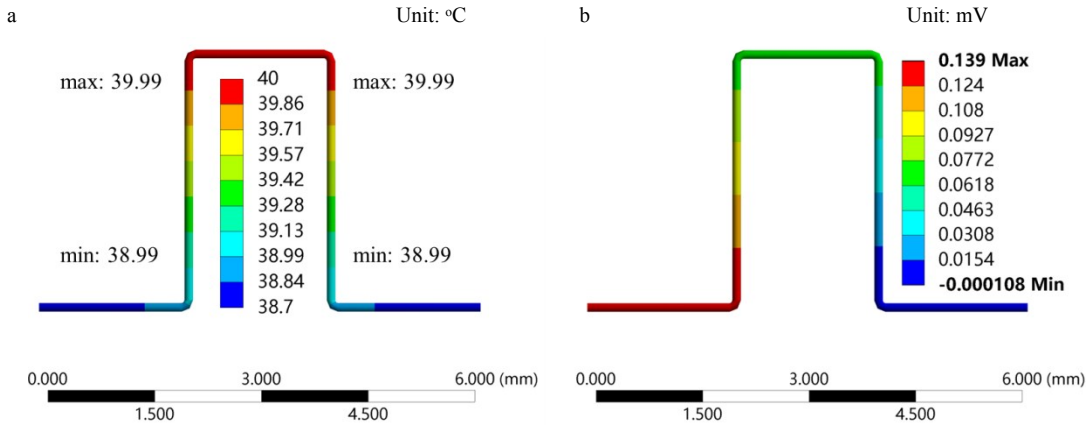

Supplementary Figure 5 | The FEA simulation results of bared single p-n pair of TEY at fixed hot-side temperature (40 °C). **a.** The temperature distribution of the bared single p-n pair of TEY. **b.** The potential distribution of bared single p-n pair of TEY.

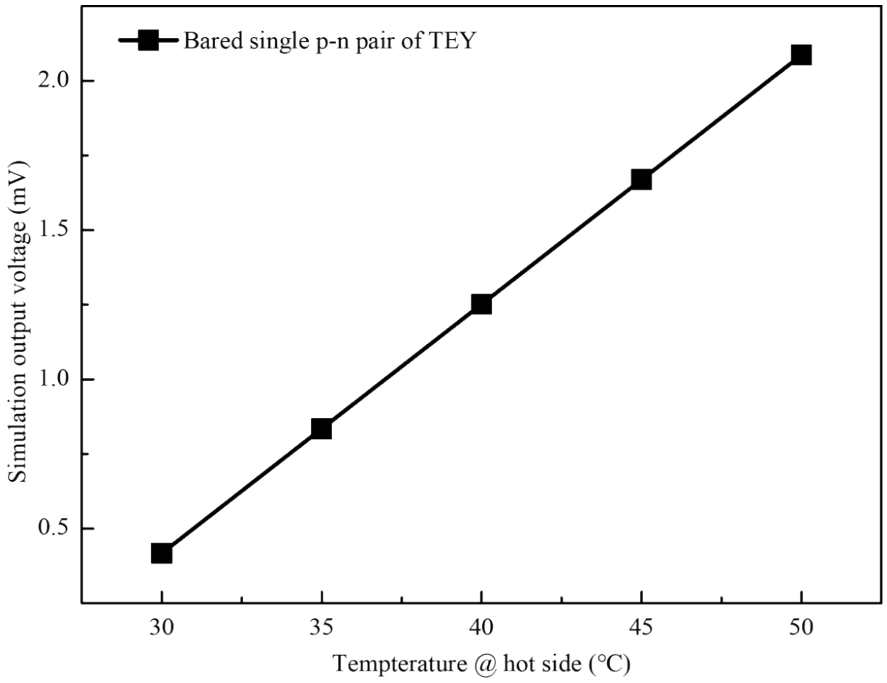

Supplementary Figure 6 | The simulated thermoelectric output voltage of bared single p-n pair of TEY.

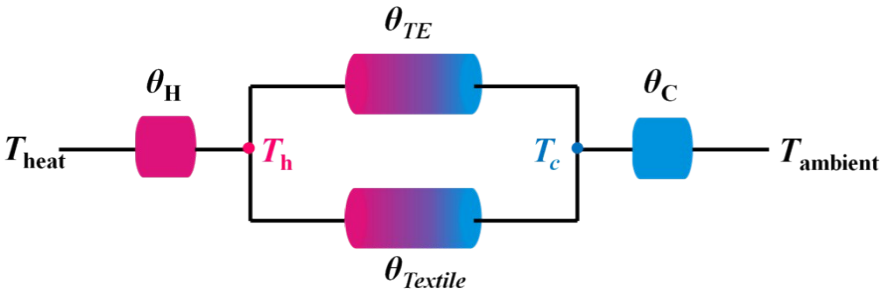

Supplementary Figure 7 | The simplified thermal resistance model.

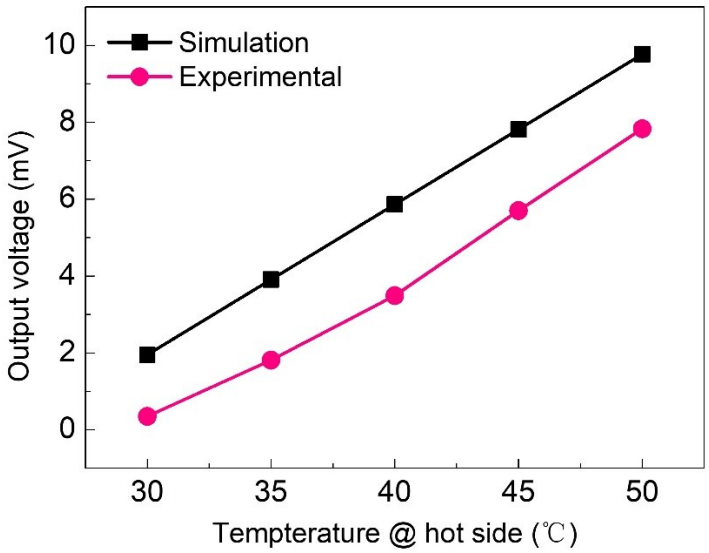

Supplementary Figure 8 | The simulation and experimental results of spacer fabric based TET.

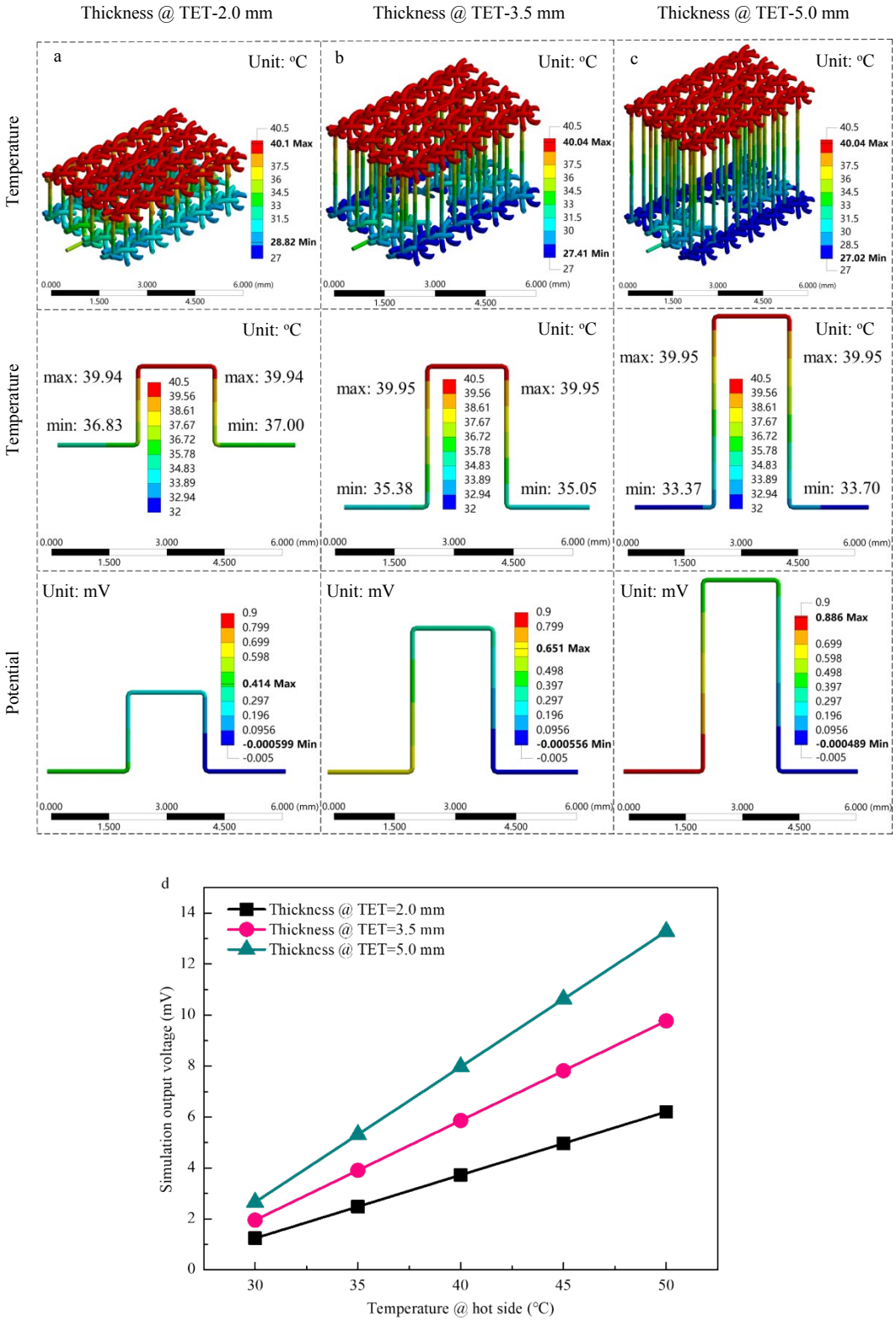

Supplementary Figure 9 | The effect of fabric thickness of spacer fabric on the thermoelectric power generation of TET.

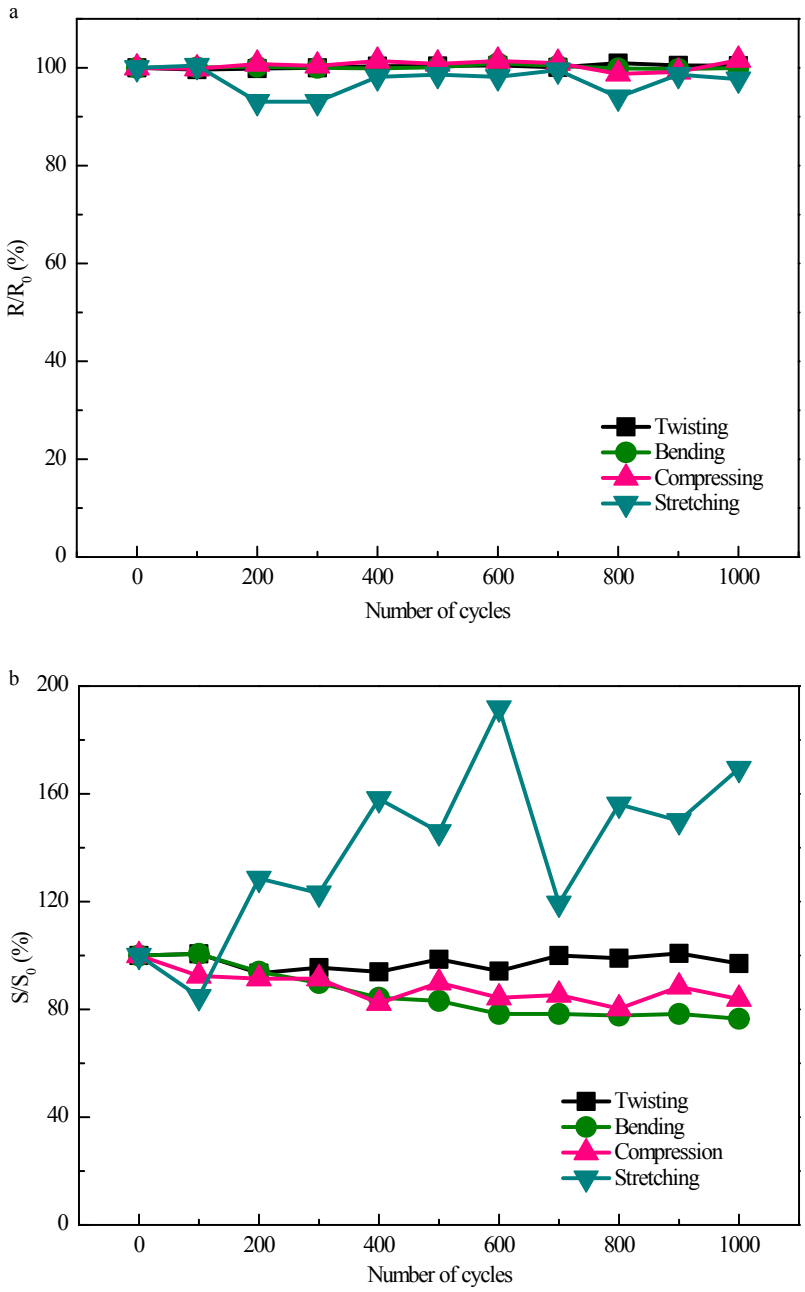

Supplementary Figure 10 | Stability of **a.** electrical conductivity and **b.** Seebeck coefficient of TET under twisting, bending, compression and stretching.

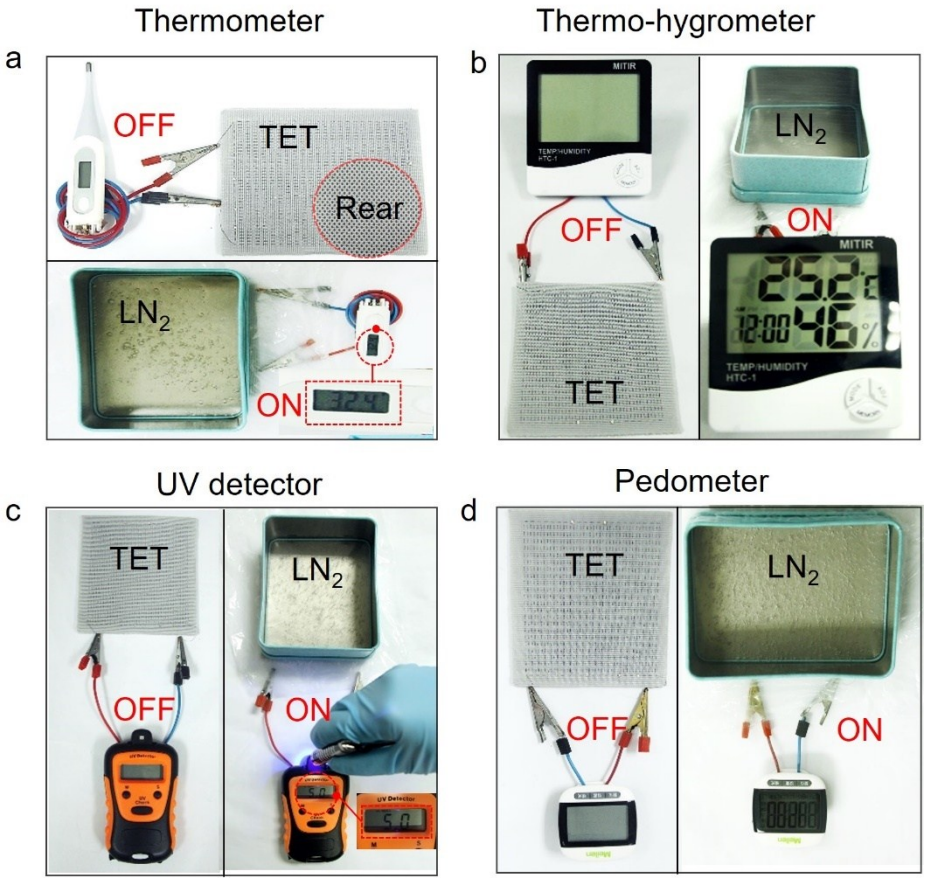

Supplementary Figure 11 | Demonstration of as-prepared TET powering several typical electronics including **a.** thermometer, **b.** thermo-hygrometer, **c.** UV detector and **d.** pedometer (ΔT~40 K).

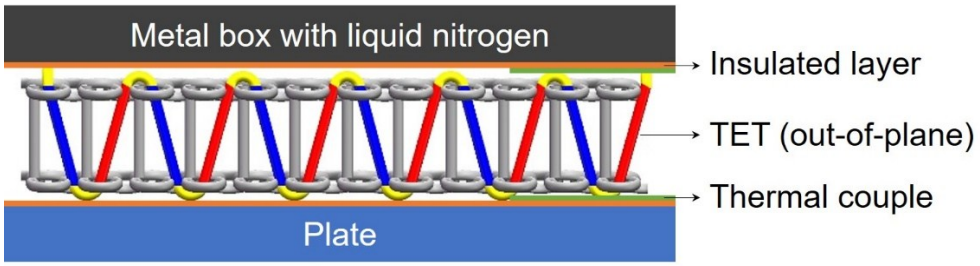

Supplementary Figure 12 | The measurement diagram of power generation during the powering electronics process (ΔT between the top and bottom surface of TET is ~40 K).

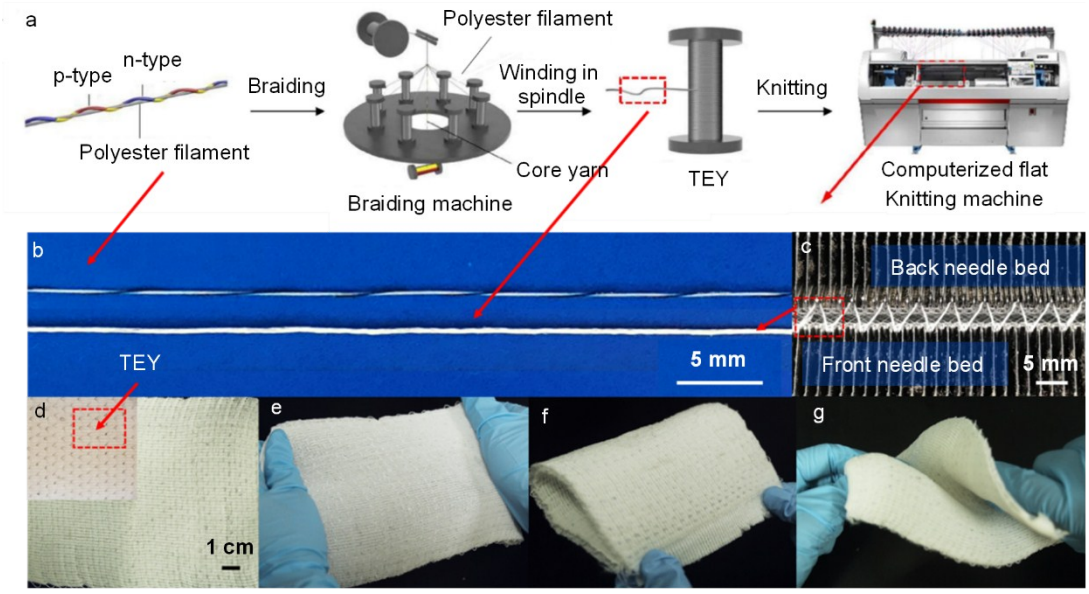

Supplementary Figure 13 | Demonstration of scalable manufacturing weft-knitted spacer fabric based TETs. **a.** Illustration of industrial weft-knitting process with a computerized flat knitting machine. The twisted core yarn comprised of TEYs with PET filaments was further braided with a fabric sheath of PET filaments to improve its anti-friction property for high-speed textile processes. A commercialized computerized flat knitting machine (Reutlingen, Germany) was used to fabricate the TET. **b.** The optical images showing the twisted TEY with thick PET filaments and core-sheath TEY. **c.** The cross-section view of braided TEYs in spacer fabric during knitting. The TEY forms a zigzag configuration in the cross-section of spacer fabric. **d.** The as-prepared spacer fabric with TEYs. The dark spots are TEY, showing uniform distribution of TEY in spacer fabric. **e-g.** The flexibility of spacer fabric shaped TET under stretching (**e**), bending (**f**) and twisting (**g**).

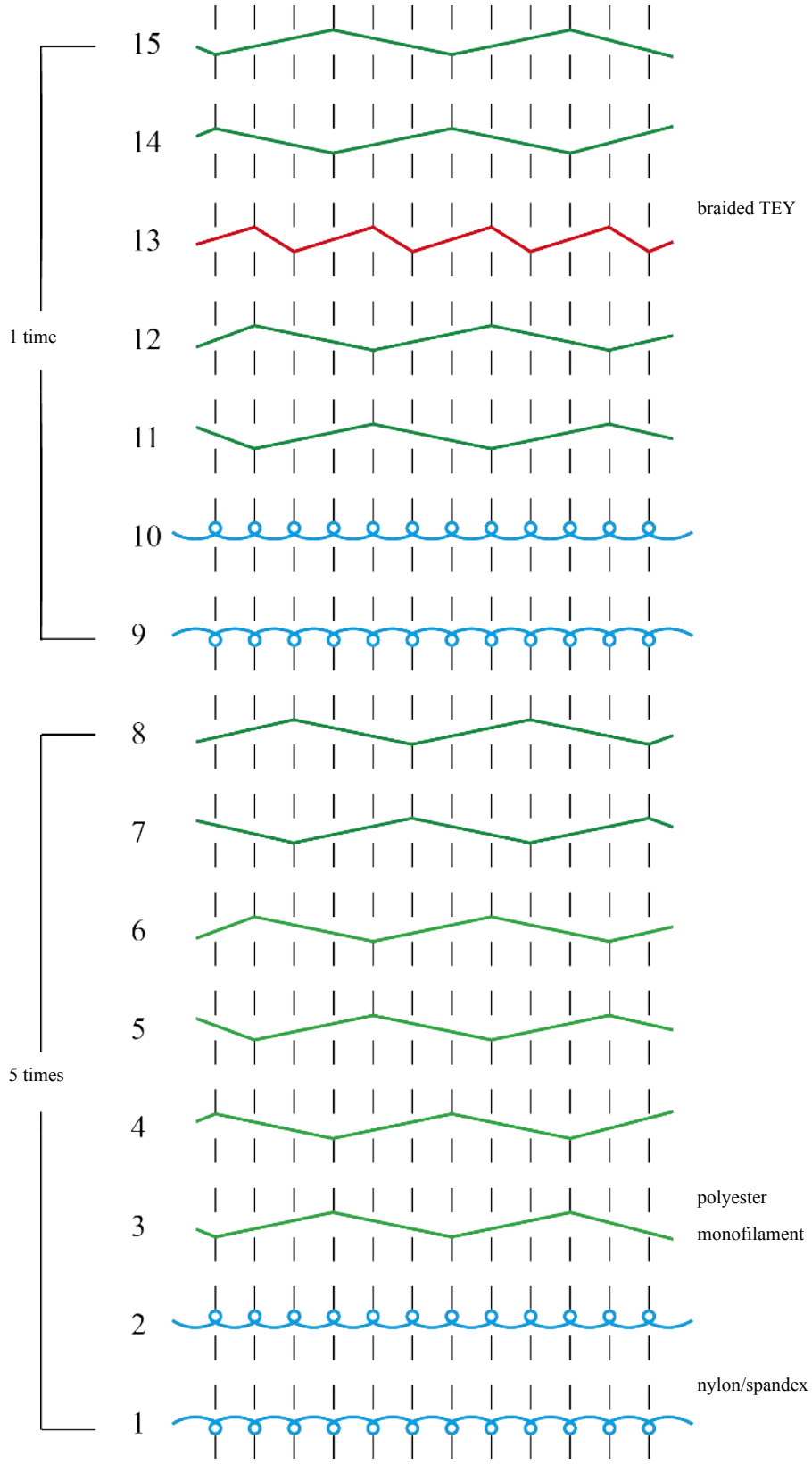

Supplementary Figure 14 | Lapping diagram of TEY and textile yarn.

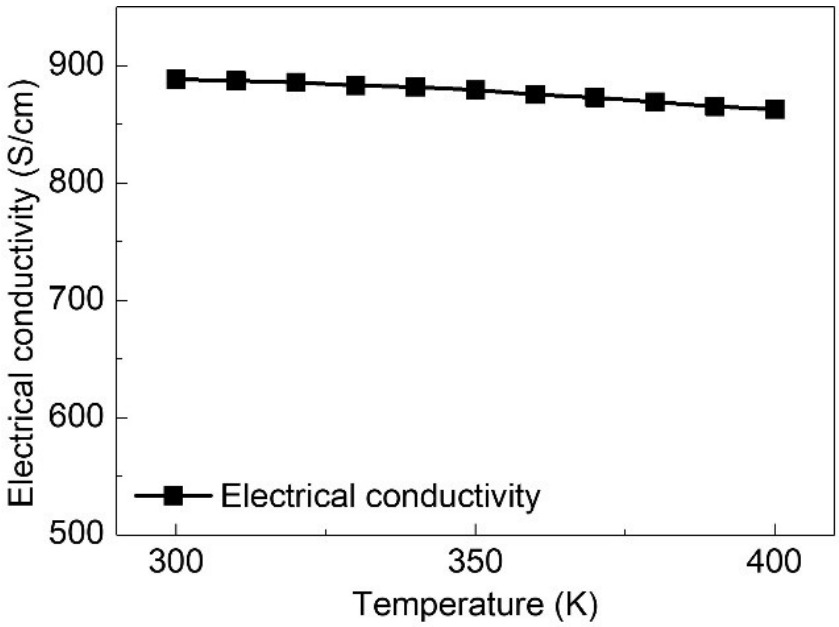

Supplementary Figure 15 | The temperature-dependent electrical conductivity of pure CNTY.

Supplementary Tables

Supplementary Table 1 Thermoelectric properties (electrical conductivity(σ), Seebeck coefficient (*S*) and power factor (PF)) of as-purchased CNTY.

Sample	Resistance (Ω)	Length (cm)	Diameter (μm)	σ (S/cm)	*S* (μV/K)	PF μW/(m·K^2)
As-purchased CNTY	4.49	0.50	122.99	938.23	55.80	292.13
	4.93	0.50	125.68	817.75	55.68	253.52
	5.08	0.50	126.40	785.17	46.26	168.02
	5.08	0.50	115.99	931.83	54.58	277.59
	4.78	0.50	136.29	717.48	57.72	239.04
Average				838.09	54.01	246.06

Supplementary Table 2 Thermoelectric properties (σ, *S* and PF) of PEDOT: PSS/CNTY.

Sample	Resistance (Ω)	Length (cm)	Diameter (μm)	σ (S/cm)	*S* (μV/K)	PF μW/(m·K^2)
PEDOT: PSS/CNTY	3.81	0.50	126.31	1047.28	69.37	503.97
	4.09	0.50	118.62	1107.04	68.84	524.62
	4.03	0.50	131.79	909.11	69.95	444.83
	4.13	0.50	117.83	1110.54	72.14	577.94
Average				1043.49	70.08	512.84

Supplementary Table 3 The comparison of thermoelectric performance of PEDOT:PSS/CNTs in our work with the thermoelectric performances of PEDOT:PSS/CNTs reported in literatures.

Type of CNT	Concentration of DMSO	S (μV/K)	σ (S/cm)	PF (μW/m K^2)	Ref
SWCNT	5 vol%	32.8	2695.1	289.0	1
SWCNT	0	18.1	359.5	10.1	2
MWCNT	0	42.1	2090.0	371.0	3
SWCNT	5 vol%	29.6	240.8	21.1	4
SWCNT	No ratio	30.0	1350.0	121.5	5
SWCNT	No ratio	28.0	3800.0	300.0	6
MWCNT	5 vol%	70.1	1043.5	512.8	This work

Supplementary Table 4 Thermoelectric properties (σ, *S* and PF) of PEI/CNTY.

Sample	Resistance (Ω)	Length (cm)	Diameter (μm)	σ (S/cm)	*S* (μV/K)	PF μW/(m·K^2)
PEI/ CNTY	3.66	0.50	115.42	1304.34	-68.64	614.53
	3.43	0.50	117.75	1339.14	-66.78	597.20
	3.70	0.50	110.25	1414.32	-69.24	678.05
	3.12	0.50	115.50	1529.10	-72.94	813.52
	3.40	0.50	113.39	1454.54	-66.10	635.52
Average				1408.29	-68.74	667.77

Supplementary Table 5 The work function (WF) of pure CNT and PEI doped CNT film.

	Cut-off edge of the secondary electrons (eV)	Work function (eV)
Pure CNT film	16.85	4.36
PEI/CNT film	17.06	4.15

Note: WF=21.21 eV-(Cut-off edge of the secondary electrons)

Supplementary Table 6 Details regarding material's parameters used in the finite element analysis.

Materials	Thermal conductivity (W/(m·K))	Electrical resistivity (ohm·cm)	Seebeck coefficient (μV/K)
Electrode (CNTY)	35.00	0.0012	/
p-type TEY	35.00	0.00096	70.08
n-type TEY	35.00	0.00071	-68.74
Insulating layer	0.20	/	/
Textile substrate	0.97	/	/

Note: We measured the thermal conductivity of CNTY by a self-heating 3ϖ method[7]. The thermal conductivities of p-type and n-type TEYs are estimated based on that of CNTY. The thermal conductivity of textile substrate is based on the reported thermal conductivity of polyester filament.

Supplementary Table 7 Boundary conditions applied in the finite element analysis.

Condition	Materials	Value
Temperature	Heating source	30-50 ^{o}C
Convection 1	Outer layer of textile substrate	10 W/(m^{2}·^{o}C)
Convection 2	Inner layer of textile substrate	0.2 W/(m^{2}·^{o}C)
Ambient temperature	/	25 ^{o}C
Voltage	A surface of one electrode	0 V

Supplementary Table 8 The thermo-wet comfortability of the as-received warped-knitted spacer fabric and warped-knitted spacer fabric shaped TET.

Sample	Air Permeability (mm/s)	Thermal resistance ($cm^2 \cdot K/W$)	Heat transfer coefficient	Clo	Insulation rate (%)
As-received warped-knitted spacer fabric	2894.00	83.52	11.97	538.80	58.36
Warp-knitted spacer fabric shaped TET	2603.00	91.62	10.91	591.10	60.59

Supplementary Table 9 The detailed data and calculating process of Fig.4i.

Table: Detailed data in References

Weight of TE materials (g)	Area of TEG (cm^2)	Output power (μW)	ΔT (K)	Output power density (μW/g K)	TEG type	Ref
17.44*a1	16.00	78.00	5.75*a2	0.78	Inorganic non-textile based	8
0.56*b1	5.59	23.00	35.00	1.18	Inorganic non-textile based	9
1.31*c1	1.50	0.22	15.00	0.011	Inorganic textile based	10
0.32*d1	17.50*d2	0.21	74.30	0.0088	Organic textile based	11
2.25*e1	36.00*e2	0.12	7.90	0.0065	Organic non-textile based	12
0.0099*f1	0.066*f2	0.72 f3	55.00	1.33	Inorganic textile-based	13
0.0099*g1	0.070*g2	0.63 g3	55.00	1.16	Inorganic textile-based	13
0.0015*h1	0.34*h2	21.21*h3	55.00	250.90	Inorganic textile-based	13
0.053*i1	36.00	0.0026	66.00	0.00075	Organic textile based	14
1.3×10^{-4}*j1	0.79*j2	0.00050	5.00	0.79	Organic textile based	15
/	3.00	/	50.00	560.00	Inorganic textile-based	16
/	3.20	/	40.00	17.43	Organic non-textile based	17
0.048	74.40	393.15	47.70	171.71	Organic textile based	This work

Note: Calculation process of the table.

*a1 Calculated data: Ref 8 presents the weight of p-type TE material is 1.02 g and the

weight of n-type TE materials is 1.16 g. There are 8 thermocouples in this TEG, so the weight of the whole TE materials is 1.12×8+1.16×8=17.44 g.

*a2 Estimated data: The data is obtained from Fig. 7b in Ref 8.

*b1 The density of p-type $Bi_{0.5}Sb_{1.5}Te_3$ is about 6.8 g/cm^3, the size of the p-type $Bi_{0.5}Sb_{1.5}Te_3$ is 1.15 mm×1.15 mm×1.2 mm, so the weight of p-type $Bi_{0.5}Sb_{1.5}Te_3$ is about 1.15×1.15×1.2÷1000×6.8=0.01079 g. The density of n-type $Bi_2Se_{0.5}Te_{2.5}$ is about 7.8 g/cm3, the size of the p-type $Bi_2Se_{0.5}Te_{2.5}$ is 1.15 mm×1.15 mm×1.2 mm, so the weight of p-type $Bi_{0.5}Sb_{1.5}Te_3$ is about 1.15×1.15×1.2÷1000×7.8=0.01238 g. There are 24 thermocouples in this TEG, so the weight of the whole TE materials is 0.01079×24+0.01238×24=0.56 g.

*c1 Estimated data: The diameter of the p-type and n-type TE materials is 4 mm and the height is 0.6 mm, so the volume is about $\pi\times2^2\times0.6$=7.54 mm^3=0.00754 cm^3. The density of p-type $Bi_{0.5}Sb_{1.5}Te_3$ is about 6.8 g/cm3, so the weight of p-type $Bi_{0.5}Sb_{1.5}Te_3$ is about 0.00754×6.8=0.0512 g. The density of n-type $Bi_2Se_{0.3}Te_{2.7}$ is about 7.73 g/cm3, so the weight of n-type $Bi_2Se_{0.3}Te_{2.7}$ is about 0.00754×7.73=0.0583 g. So the total weight of TE materials is 0.0512×12+0.0583×12=1.31 g.

*d1 Estimated data: The size of each cotton TE strip is 35 mm×5 mm, the area density of the cotton TE strip is assumed to be 0.037 g/cm^2. There are 5 strips, so the total weight of the TE legs is about 3.5×0.50.037×5=0.32 g.

*d2 Estimated data: The data is obtained from Fig. 3b in Ref 11.

*e1 Estimated data: The size of the p-type film is 18 mm×2 mm×600 nm and the density

of the film is assumed to be 1.01 g/cm^3. So the weight of the p-type film is about $1.8\times0.2\times600\times10^{-7}\times1.01=2.1816\times10^{-5}$ g. The size of the n-type Bi_2Te_3 is 2 mm×2 mm×2 mm and the density of it is about 7.8 g/cm^3. So the weight of n-type leg is $0.2\times0.2\times0.2\times7.8=0.0624$ g. There are 36 thermocouples, so the total weight of TE materials is $2.1816\times10^{-5}\times36+0.0624\times36=2.25$ g.

*e2 Estimated data: The data is obtained from Fig. 1b in Ref 12.

*f1 Estimated data: The area density of the n- or p-type sheets was about 0.15 mg/cm^2, the size of each PAN sheet can be estimated to be 4.5 cm×1.22 cm from Fig. 2a. There are 6 PAN sheets in this fabric, so the total weight of the TEG is $0.15\times2\times4.5\times1.22\div1000\times6=0.0099$ g.

*f2 Calculated data: Ref 13 presents the output power of per couple is 0.24 μW and the power density is 0.11 W/m^2. There are 3 TE couples. So the area of TEG is $0.24\times3\div(0.11\times10^6)\times10^4=0.066$ cm^2.

*f3 Estimated data: Ref 13 presents the output power of per couple is 0.24 μW. There are 3 TE couples. So the output power of the TEG is $0.24\times3=0.72$ μW.

*g1 Estimated data: This is the same as data*f1.

*g2 Calculated data: Ref 13 presents the output power of per couple is 0.21 μW and the power density is 0.09 W/m^2. There are 3 TE couples. So the area of TEG is $0.21\times3\div(0.09\times10^6)\times10^4=0.070$ cm^2.

*g3 Estimated data: Ref 13 presents the output power of per couple is 0.21 μW. There are 3 TE couples. So the output power of the TEG is $0.21\times3=0.63$ μW.

*h1 Estimated data: The length of each p/n segment in the TE twisted yarn can be

estimated to be 1 mm from Fig. 2b in Ref 13. There are 21 thermocouples in this plain-weave fabric. So the total length of the TE part is 1×21×2=42 mm. The width of the PAN sheet is about 1.22 cm. The area density of the n- or p-type sheets was about 0.15 mg/cm^2. So the total weight of TE materials is about 4.2×1.22×0.15×2÷1000=0.0015 g.

*h2 Calculated data: Ref 13 presents the output power of per couple is 1.01 μW and the power density is 0.62 W/m^2. There are 21 TE couples. So the area of TEG is 1.01×21÷(0.62×10^6)×10^4=0.34 cm^2.

*h3 Estimated data: Ref 13 presents the output power of per couple is 1.01 μW. There are 21 TE couples. So the output power of the TEG is 1.01×21=21.21 μW.

*i1 Estimated data: The length of the whole polyester TE yarn is estimated to be 3.58 m according to the Fig. 3. The density of the polyester TE yarn is assumed to be 14.7625 g/km. So the total weight of TE yarn is about 3.58×14.7625÷1000=0.053 g.

*j1 Estimated data: The length of the whole CNT TE yarn is estimated to be 8.38 cm according to the Fig. 3. The diameter of the CNT yarn is 40 μm. The density of the CNT yarn is assumed to be 1.2 g/cm^3. So the total weight of the TE material is about $\pi\times(2\times10^{-3})^2\times8.38\times1.2=1.3\times10^{-4}$ g.

*j2 Estimated data: The data is obtained from Fig. 5b in Ref 15.

Supplementary References

1. S. Liu, H. Li and C. He, *Carbon*, 2019, **149**, 25-32.

2. J. Y. Kim, W. Lee, Y. H. Kang, S. Y. Cho and K. S. Jang, *Carbon*, 2018, **133**, 293-299.

3. W. Lee, Y. H. Kang, J. Y. Lee, K. S. Jang and S. Y. Cho, *Mater. Today Commun.*, 2017, **10**, 41-45.

4. H. Song, C. Liu, J. Xu, Q. Jiang and H. Shi, *RSC Adv.*, 2013, **3**, 22065-22071.

5. C. Yu, K. Choi, L. Yin and J. C. Grunlan, *ACS Nano*, 2011, **5**, 7885-7892.

6. L. Zhang, Y. Harima and I. Imae, *Org. Electron.*, 2017, **51**, 304-307.

7. Y. Sun, L. Qiu, L. Tang, H. Geng, H. Wang, F. Zhang, D. Huang, W. Xu, P. Yue, Y. Guan, F. Jiao, Y. Sun, D. Tang, C. Di, Y. Yi and D. Zhu, *Adv. Mater.*, 2016, **28**, 3351-3358.

8. H. Park, D. Kim, Y. Eom, D. Wijethunge, J. Hwang, H. Kim and W. Kim, *J. Phys. D Appl. Phys.*, 2017, **50**.

9. Y. Shi, Y. Wang, D. Mei, B. Feng and Z. Chen, *IEEE Robot. Autom. Lett.*, 2018, **3**, 373-378.

10. M. K. Kim, M. S. Kim, S. Lee, C. Kim and Y. J. Kim, *Smart Mater. Struct.*, 2014, **23**, 105002.

11. Y. Du, K. Cai, S. Shen, R. Donelsonand, J. Xu, H. Wang and T. Lin, *RSC Adv.*, 2017, **7**, 43737-43742.

12. T. Park, H. Lim, J. U. Hwang, J. Na, H. Lee and E. Kim, *APL Mater.*, 2017, **5**, 074106.

13. J. A. Lee, A. E. Aliev, J. S. Bykova, M. J. de Andrade, D. Kim, H. J. Sim, X. Lepro, A. A. Zakhidov, J. B. Lee, G. M. Spinks, S. Roth, S. J. Kim and R. H. Baughman, *Adv. Mater.*, 2016, **28**, 5038-5044.

14. Q. Wu and J. Hu, *Smart Mater. Struct.*, 2017, **26**, 045037.

15. M. Ito, T. Koizumi, H. Kojima, T. Saito and M. Nakamura, *J. Mater. Chem. A*, 2017, **5**, 12068-12072.

16. S. J. Kim, J. H. We and B. J. Cho, *Energy Environ. Sci.*, 2014, **7**, 1959.

17. J. Choi, Y. Jung, S. J. Yang, J. Y. Oh, J. Oh, K. Jo, J. G. Son, S. E. Moon, C. R. Park and H. Kim, *ACS Nano*, 2017, **11**, 7608-7614.